Catalysis Communications 75 (2016) 1–5

Contents lists available at ScienceDirect

Catalysis Communications

journal homepage: www.elsevier.com/locate/catcom

Short communication

Vapor phase esterification of levulinic acid over ZrO_2/SBA-15 catalyst

E. Siva Sankar, V. Mohan, M. Suresh, G. Saidulu, B. David Raju, K. S. Rama Rao *

Inorganic and Physical Chemistry Division, CSIR-Indian Institute of Chemical Technology, Hyderabad, India 5000071

ARTICLE INFO

Article history:
Received 29 July 2015
Received in revised form 15 September 2015
Accepted 5 October 2015
Available online 8 October 2015

Keywords:
ZrO_2/SBA-15
Esterification
Levulinic acid
Alkyl levulinate
γ-valerolactone
MPV reduction

ABSTRACT

ZrO_2/SBA-15 catalysts with different ZrO_2 loadings prepared by impregnation method were tested for the esterification of levulinic acid in a fixed-bed reactor in vapor phase conditions at atmospheric pressure for the first time and found that the catalyst with 7 weight percent ZrO_2 exhibited 100% conversion of levulinic acid and 96% selectivity to methyl levulinate due to the presence of more number of moderate acidic sites. It is interesting to observe the formation of γ-valerolactone as the alcohol chain length increases at the expense of alkyl levulinate, through MPV reduction mechanism.

1. Introduction

Levulinic acid is an inexpensive renewable resource, obtained through the acid hydrolysis of pentose's and hexoses [1,2], and is considered as a promising chemical for the production of chemicals, fuels, and fuel additives. This molecule has been the subject of focus in recent times owing to presence of both highly reactive functional groups [1,3–5]. In recent times, catalytic transformations of levulinic acid to valuable compounds including alkyl levulinate, γ-valerolactone, and others have been extensively reported [2,5–10]. To obtain these valuable compounds, various methods like hydrogenation, esterification, reductive amination, oxidation, etc., can be applied. Among, esterification of levulinic acid seems to be important because the compounds synthesized through this methodology find applications in flavoring agents, plasticizers, solvents, and fragrances, etc., and as fuel additives [6–9]. The esterification of levulinic acid has been commonly performed in presence of inorganic acids like H_2SO_4 [9–14]. The disadvantages associated with the use of inorganic acids are their corrosiveness, lack of recyclability, and separation problems after the reaction. In this scenario, many groups tried the application of solid acids such as heteropoly acids, zeolites, and sulphated metal oxides for the esterification of levulinic acid [6–9]. Most of the catalysts for the esterification of levulinic acid were operated in batch conditions. In this scenario, there is room for the design and development of heterogeneous catalysts for the continuous processes. The advantages of continuous process are no solvent usage, ease of catalyst separation, and can be operated for longer hours. Herein, we report esterification of levulinic acid over mesoporous ordered SBA-15 supported ZrO_2 catalysts in vapor phase at atmospheric pressure.

2. Experimental

2.1. Catalyst preparation

SBA-15 designated hereafter as 'S' was synthesized using a procedure described elsewhere [15,16,17]. The synthesized SBA-15 was used as a support for the preparation of ZrO_2/SBA-15 catalyst. ZrO_2/SBA-15 catalysts with various zirconia loadings were prepared by impregnation method using zirconium acetyl acetonate as a precursor. These catalysts were designated as 3ZS, 7ZS, and 10ZS, respectively, where the numerical stands for the weight percent of ZrO_2. The composition of ZrO_2 was calculated by using ICP-OES iCAP6500 DU (M/s.Thermo Scientific, USA) instrument.

2.2. Catalyst characterization

Textural properties of SBA-15, ZrO_2, and ZrO_2/SBA-15 catalysts were measured by means of nitrogen adsorption and desorption measurements at liquid nitrogen temperature on a Quadrasorb SI system (M/s. Quantachrome Instruments, USA). BJH method was applied to get the pore size distributions. Structural characterization was obtained on an Ultima IV X-ray powder diffractometer (M/s. Rigaku Corporation, Japan), with a scanning step of 0.02° using Ni-filtered Cu Kα radiation (λ = 1.5406 Å) with a scan speed of 4° min^{-1} and a scan range of 10–80° at 40 kV and 20 mA. The detailed characterizations of the catalysts were described in electronic supplementary material.

* Corresponding author.
E-mail addresses: ksramarao@iict.res.in, ksramarao.iict@gov.in (K.S. Rama Rao).

http://dx.doi.org/10.1016/j.catcom.2015.10.013
1566-7367/

2.3. Catalytic activity

The vapor phase esterification was performed in fixed-bed quartz reactor (14 mm id and 300 mm long) at atmospheric pressure. 0.5 g of the catalyst and same amount of the quartz particles were mixed and loaded at the center of the quartz reactor and flushed at 523 K for 1 h in N_2 flow of 1800 cm^3h^{-1}. The liquid feed with required molar ratios of LA and alcohol (1: 7) (unless specified) were continuously fed at a flow rate of 1 cm^3h^{-1} (unless specified) using a syringe pump (M/s. B. Braun, Germany). The product mixture was collected in an ice-cooled trap at regular intervals and analyzed by a FID equipped GC-17A (M/s. Shimadzu Instruments, Japan) with EB–5 capillary column (30 m × 0.53 mm × 5.0 μm) and confirmed by GC-MS, QP-5050 (M/s. Shimadzu Instruments, Japan) with EB–5 M/s. capillary column (30 m × 0.25 mm × 0.25 μm).

3. Results and discussion

3.1. X-ray diffraction analysis

XRD patterns of SBA-15 and ZrO_2/SBA-15 catalysts (Fig. 1) exhibited a well-resolved pattern with a sharp reflection at a 2θ value of around 0.9° and another two weak peaks at around 1.6° and 1.7°, which are in line with the earlier reports [15,18]. The intensities of these peaks are found to decrease as ZrO_2 loading increases. The estimated unit cell parameters of a hexagonal lattice, d (100), are shown in Table 1. Interestingly, larger unit cell parameters are observed for the ZrO_2-incorporated amples which may be due to the incorporation of ZrO_2 species into the framework of mesoporous SBA-15 [19,20]. Reflections due to ZrO_2 are absent in the wide angle XRD patterns (inset of Fig. 1) indicating the amorphous nature of ZrO_2 in all the ZrO2/SBA-15 catalysts. In order to confirm the presence of ZrO_2, these catalysts were subjected to ICP-OES and found 2.7, 6.8, and 9.3 weight percent of ZrO_2 in 3ZS, 7ZS, and 10ZS catalysts, respectively, which clearly indicates the closeness of ZrO_2 content with the theoretical values.

3.2. Nitrogen adsorption–desorption studies

N_2 adsorption–desorption isotherms of SBA-15 and ZrO_2/SBA-15 catalysts are shown in Fig. 2. All the N_2 adsorption–desorption isotherms except parent ZrO_2 are found to be of Type IV in nature as per the IUPAC classification and show evidence of an H1 hysteresis loop corresponding to mesoporous solids [21]. Besides, the adsorption branches of isotherm demonstrated a sharp inflection at a relative pressure of 0.7 < P/P0 < 0.85, which is due to the capillary condensation in the ordered mesopores [22]. Furthermore, the position of the inflection point is obviously associated to a diameter in the mesopore range, and the sharpness of these steps specifies the evenness of the mesopore size distribution [22,23]. The pore size distribution curves (inset of Fig. 2) indicates that majority of the pores are concentrated at around 7 nm even though this value is different from the average pore size (~6 nm). Generally, the pore wall thickness of SBA-15 type mesoporous materials will be lower than average pore size, but there are instances where both values are more or less same [24–26].

Table 1
Physico-chemical properties of ZrO_2/SBA-15 catalysts.

Catalyst	S_{BET}[a] (m^2/g)	D_p[b] (nm)	V_p[c] (cc/g)	d_{100}[d] nm	a_0[e]	$t^f = a_o - D_p$
S	715	5.60	1.01	9.20	10.62	5.02
3ZS	712	5.59	1.09	9.79	11.31	5.72
7ZS	701	5.57	0.97	9.75	11.26	5.69
10ZS	663	5.86	0.94	9.89	11.42	5.56
ZrO_2	32	8.79	0.08	-	-	-

[a] BET surface area.
[b] Average pore size.
[c] Total pore volume.
[d] Periodicity of SBA-15 derived from a low-angle XRD.
[e] Unit cell length.
[f] Pore wall thickness.

3.3. UV–Vis diffuse reflectance spectroscopy (UV–Vis-DRS)

The UV–vis-DRS patterns of ZrO_2/SBA15 catalysts (ES1) show an absorption band in the range of 205–215 nm [20,26–30]. This absorption band could be ascribed to ligand-to-metal charge transfer (LMCT, i.e., from an O^{2-} to an isolated Zr^{4+} ion in a tetrahedral configuration). This peak is due to the presence of isolated Zr^{4+} ions in the SBA-15 mesoporous framework [20]. In addition, a diverse broad band of low intensity at ~280 nm was observed in all the ZrO_2/SBA15 samples which might be due to the highly distributed ZrO_2 nanoparticles [24, 25,29]. Furthermore, an additional band in the vicinity of 230 nm appeared in the UV–vis-DRS patterns of 7ZS and 10ZS samples could be ascribed to the presence of bigger ZrO_2 particles (may be below the XRD detection limit) in these samples [26,27,30].

3.4. Temperature-programmed desorption of ammonia

From the temperature-programmed desorption of ammonia profiles of the catalysts (ES 2), the acid site population can be classified as weak (<523 K), medium (523–673 K), and strong (>673 K) acidic sites [5]. ZrO_2 possesses very strong acid sites. The strong acid peak identified

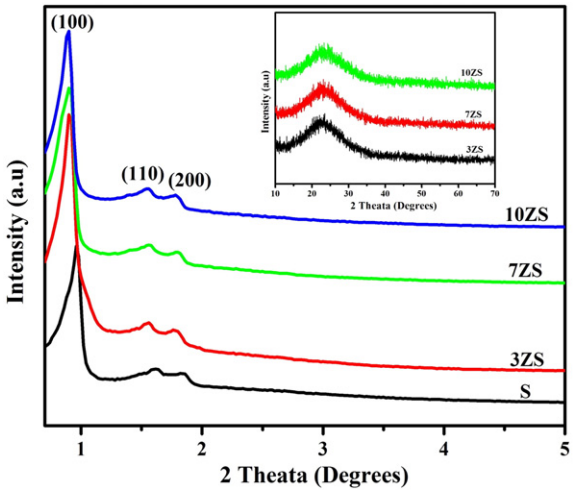

Fig. 1. Low-angle XRD pattern of parent SBA-15 and ZrO_2/SBA-15 and in inset figure wide-angle XRD patterns of ZrO_2/SBA-15.

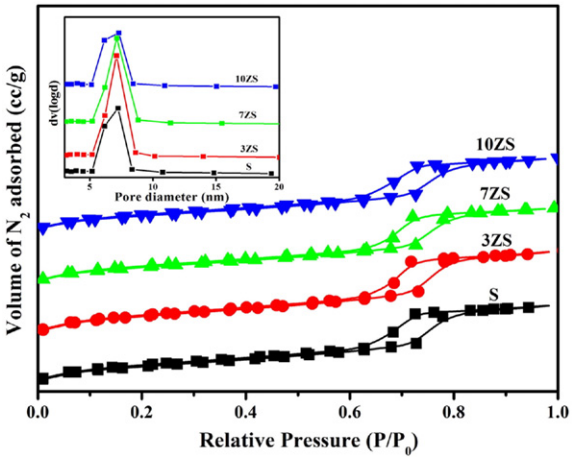

Fig. 2. N_2 adsorption–desorption isotherms for parent SBA-15 and various ZrO_2/SBA-15 samples and in inset figure pore size distribution of parent SBA-15 and various ZrO_2/SBA-15.